Open Access Full Text Article

ORIGINAL RESEARCH

Physiologically based pharmacokinetic modeling of zinc oxide nanoparticles and zinc nitrate in mice

Wei-Yu Chen[1]
Yi-Hsien Cheng[2]
Nan-Hung Hsieh[3]
Bo-Chun Wu[2]
Wei-Chun Chou[4]
Chia-Chi Ho[4]
Jen-Kun Chen[5]
Chung-Min Liao[2,*]
Pinpin Lin[4,*]

[1]Department of Biomedical Science and Environmental Biology, Kaohsiung Medical University, Kaohsiung, [2]Department of Bioenvironmental Systems Engineering, National Taiwan University, Taipei, [3]Institute of Labor, Occupational Safety and Health, Ministry of Labor, New Taipei City, [4]National Institute of Environmental Health Sciences, [5]Institute of Biomedical Engineering and Nanomedicine, National Health Research Institutes, Zhunan, Taiwan

*These authors contributed equally to this work

Correspondence: Chung-Min Liao
Department of Bioenvironmental Systems Engineering, National Taiwan University, Number 1, Section 4, Roosevelt Road, Taipei 10617, Taiwan
Tel +886 2 2363 4512
Email cmliao@ntu.edu.tw

Pinpin Lin
National Institute of Environmental Health Sciences, National Health Research Institutes, Keyan Road, Zhunan, Miaoli County 35053, Taiwan
Tel +886 37 246 166 ext 36508
Fax +886 37 587 406
Email pplin@nhri.org.tw

Abstract: Zinc oxide nanoparticles (ZnO NPs) have been widely used in consumer products, therapeutic agents, and drug delivery systems. However, the fate and behavior of ZnO NPs in living organisms are not well described. The purpose of this study was to develop a physiologically based pharmacokinetic model to describe the dynamic interactions of ^{65}ZnO NPs in mice. We estimated key physicochemical parameters of partition coefficients and excretion or elimination rates, based on our previously published data quantifying the biodistributions of 10 nm and 71 nm ^{65}ZnO NPs and zinc nitrate (^{65}Zn(NO$_3$)$_2$) in various mice tissues. The time-dependent partition coefficients and excretion or elimination rates were used to construct our physiologically based pharmacokinetic model. In general, tissue partition coefficients of ^{65}ZnO NPs were greater than those of ^{65}Zn(NO$_3$)$_2$, particularly the lung partition coefficient of 10 nm ^{65}ZnO NPs. Sensitivity analysis revealed that 71 nm ^{65}ZnO NPs and ^{65}Zn(NO$_3$)$_2$ were sensitive to excretion and elimination rates in the liver and gastrointestinal tract. Although the partition coefficient of the brain was relative low, it increased time-dependently for ^{65}ZnO NPs and ^{65}Zn(NO$_3$)$_2$. The simulation of ^{65}Zn(NO$_3$)$_2$ was well fitted with the experimental data. However, replacing partition coefficients of ^{65}ZnO NPs with those of ^{65}Zn(NO$_3$)$_2$ after day 7 greatly improved the fitness of simulation, suggesting that ZnO NPs might decompose to zinc ion after day 7. In this study, we successfully established a potentially predictive dynamic model for slowly decomposed NPs. More caution is suggested for exposure to ^{65}ZnO NPs <10 nm because those small ^{65}ZnO NPs tend to accumulate in the body for a relatively longer time than 71 nm ^{65}ZnO NPs and ^{65}Zn(NO$_3$)$_2$ do.

Keywords: zinc nanomaterials, bioaccumulation, biodistribution, PBPK modeling, partition coefficient

Introduction

Nanomaterials have a broad range of applications in technology and biological medicine because of the unique properties of nanoparticles (NPs), which render nanomaterials convenient and efficient for use. However, the increasing use of engineered NPs has led to increased exposure potential and concern for human and environmental safety. NPs can enter an organism through various pathways and distribute systemically in the circulatory and lymphatic systems and ultimately into tissues.[1] The biodistribution of NPs might markedly influence their biological effects in vivo, such as in inflammatory and oxidative responses related to cardiopulmonary toxicity.[2,3]

Zinc oxide nanoparticles (ZnO NPs) are commonly used in sunscreens in particle sizes ranging from 70 nm to 100 nm because of strong ultraviolet absorptive properties. ZnO NPs also have potential application in the delivery of therapeutic agents for tumors and autoimmune diseases.[4–6]

In our previous study, we reported the biodistribution of ^{65}ZnO NPs in mice.[7] The results provide relevant data for developing a particle size-dependent physiologically

based pharmacokinetic (PBPK) model for metal NPs. The advantages of a PBPK model include the ability to integrate the physiological structures of organisms and the physicochemical properties of toxicants and provide quantitative descriptions of the kinetic processes of absorption, distribution, metabolism, and excretion.[8] A PBPK model is an effective tool to estimate the time course of chemical accumulation in target tissues of organisms and can be incorporated into a quantitative risk assessment framework. The dynamic interactions of NPs in living organisms, such as transportation kinetics across biobarriers, can also be described by a metal NP-based PBPK model. A nanometal PBPK model with adequate predictive power can be used to investigate mechanical processes, evaluate hypotheses, and guide experimental designs and also has advantages of reduced animal testing and costs and the ability to simulate and predict biodistribution in humans and the human response to NPs.[9]

Therefore, in this study, we aimed to develop an appropriate particle size-dependent PBPK model for describing ^{65}ZnO NP pharmacokinetics in mice and to evaluate the tissue accumulation properties of various ^{65}ZnO NP sizes and zinc nitrate (^{65}Zn(NO$_3$)$_2$). We identified that physicochemical parameters of 10 nm and 71 nm ^{65}ZnO NPs and ^{65}Zn(NO$_3$)$_2$ in NP PBPK modeling were predictive of ^{65}ZnO NP biodistribution and accumulative levels in living organisms. Our PBPK model was able to predict the distributions of ^{65}ZnO NPs and ^{65}Zn(NO$_3$)$_2$ in target tissues.

Materials and methods

All animal treatments and experimental protocols for this study were reviewed and approved by the Institutional Animal Care and Use Committee of the National Health Research Institutes (NHRI), Zhunan, Taiwan.

Test NPs

ZnO NPs of 71 nm diameter were purchased from Alfa Aesar (Ward Hill, MA, USA), while ZnO NPs of 10 nm diameter were purchased from NanoScale Corporation (Manhattan, KS, USA). Zn(NO$_3$)$_2$ was purchased from Showa Corporation (Tokyo, Japan). Radioactive ^{65}ZnO NPs and ^{65}Zn(NO$_3$)$_2$ were generated using the Tsing Hua Open-Pool Reactor (THOR; National Tsing Hua University, HsinChu, Taiwan). Before neutron activation, the surface area, surface charge, shape, and size distribution of cold ZnO NPs were assessed and reported in the previously published paper.[7]

For surface chemistry identification, ZnO NPs were subjected to Raman spectroscopic analysis using DXR Raman Microscope (DXR; Thermo Fisher Scientific, Waltham, MA, USA) with DXR 532 nm laser and full-range grating (50–3,500 cm^{-1}). For crystalline analysis, each sample (1 g) was filled into a sample holder and subjected to X-ray powder diffraction. The measurements were carried out by powder X-ray diffraction (MiniFlex II, Rigaku Corporation, Tokyo, Japan) with a scan speed of 2° per minute for the scan angle between 10° and 90°. Figure S1A and B are Raman spectra of 10 nm and 71 nm ZnO NPs, respectively, in which the characteristic Zn–O stretching bands are observed at 436 cm^{-1} and both NPs are not chemically modified on their surface.[10] Figure S2A and B display X-ray diffraction patterns of 10 nm and 71 nm ZnO NPs, respectively, presenting no significant difference between these two NPs. The diffraction peaks for 10 nm ZnO NPs are located at 31.62°, 34.30°, 36.12°, 47.42°, 56.46°, 62.84°, 65.32°, 67.84°, and 69.00°. The diffraction peaks for 71 nm ZnO NPs are located at 31.44°, 34.10°, 35.92°, 47.24°, 56.28°, 62.54°, 65.12°, 67.64°, and 68.78°. These X-ray diffraction patterns are assigned to (100), (002), (101), (102), (110), (103), (200), (112), and (201) planes of hexagonal wurtzite crystal of ZnO, which are in good agreement with data published by Talam et al and Uysala et al.[11,12]

Study data

Using previously published tissue accumulation data from mice injected with ^{65}ZnO NPs and ^{65}Zn(NO$_3$)$_2$, the size-dependent ^{65}ZnO NP and ^{65}Zn(NO$_3$)$_2$ PBPK mice model were constructed.[7] The experiments provided information on tissue burdens that enabled intravenously injected ^{65}ZnO NPs and ^{65}Zn(NO$_3$)$_2$ to be compared. Before neutron activation, the surface area, surface charge, shape, and size distribution of cold ZnO NPs were assessed and reported in the previously published paper.[7]

To evaluate the accumulation of 10 nm and 71 nm ^{65}ZnO NPs and ^{65}Zn(NO$_3$)$_2$, 120 μg of suspended ^{65}ZnO NPs or ^{65}Zn(NO$_3$)$_2$ were dissolved in 400 μL of distilled water and injected into 6-week-old male ICR mice (0.031–0.032 kg) through a tail vein.[7] The sampling times for accumulation and tissue weight measurements were 1, 2, 4, and 7 hours and 1, 2, 3, 7, and 28 days postinjection. The tissue samples included blood, liver, lung, kidney, spleen, brain, heart, gastrointestinal (GI) tract, and carcass (muscle and bone).

Model construction

Figure 1 shows the study framework and computational algorithm. The prototypical mice PBPK model for ^{65}ZnO NPs and ^{65}Zn(NO$_3$)$_2$ (Figure 2) were established based on the key assumptions that 1) a chemical is well mixed and homogeneously distributed within each compartment, 2) all transport within blood and tissues is limited by the flow circulatory
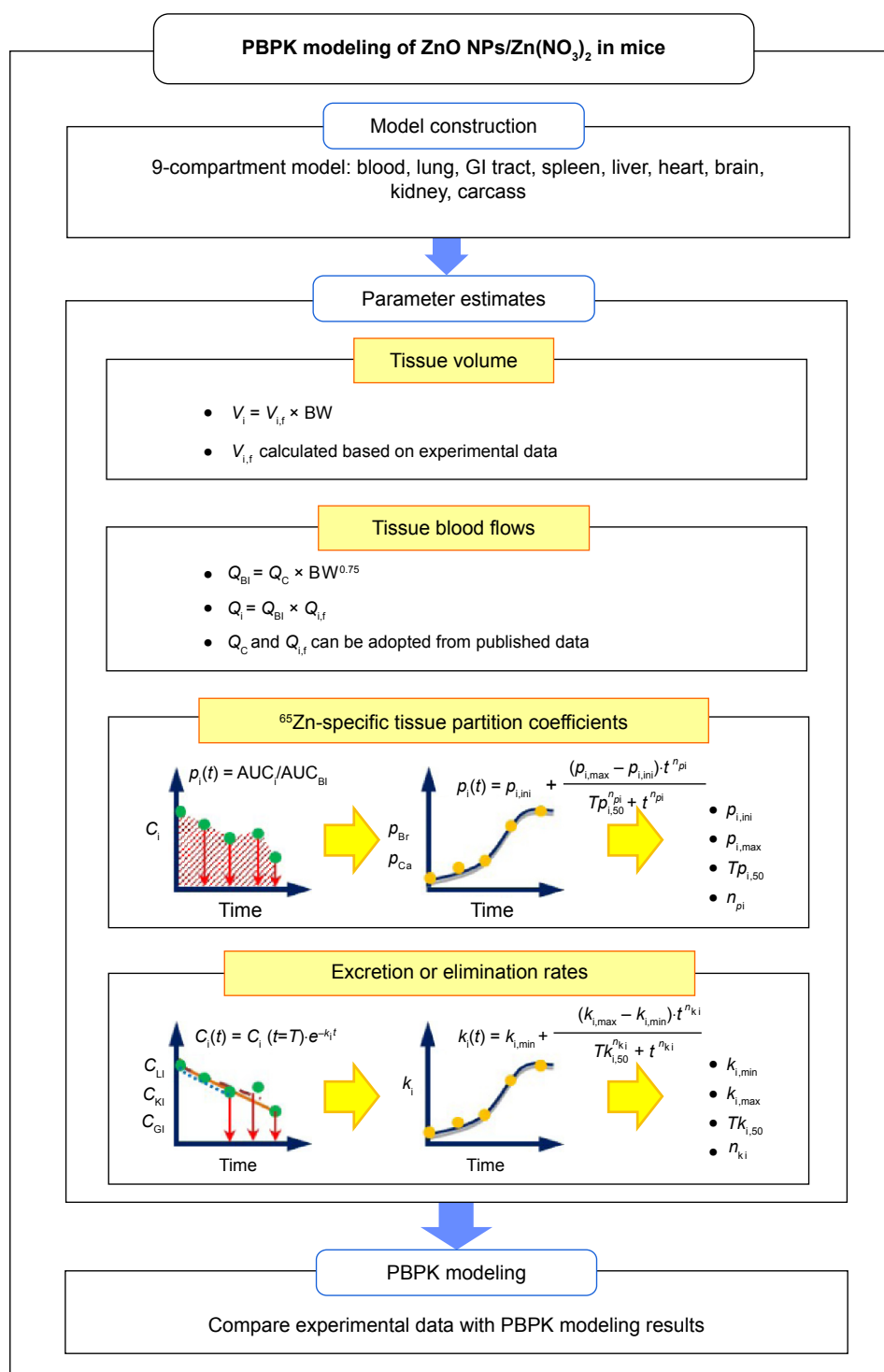
Figure 1 Schematic of the study framework and computational algorithm.
Abbreviations: V_i, tissue volume; $V_{i,f}$, percentage tissue volume; BW, body weight; Q_{Bl}, cardiac output rate; Q_C, cardiac output constant; Q_i, tissue-specific output rate; $Q_{i,f}$, percentage cardiac output rate; $p_i(t)$, partition coefficient at time t; AUC_i and AUC_{Bl}, area under the curve of each tissue and blood, respectively; $p_{i,ini}$, initial value of p_i; $p_{i,max}$, maximum value of p_i; $Tp_{i,50}$, time to reach half maximum p_i; n_{pi}, Hill coefficient of p_i; $C_i(t)$, tissue-specific concentration at time t; C_i ($t=T$), tissue-specific concentration estimated by specific time T; $k_i(t)$, excretion or elimination rate at time t; $k_{i,min}$, minimum value of k_i; $k_{i,max}$, maximum value of k_i; $Tk_{i,50}$, time to reach half maximum k_i; n_{ki}, Hill coefficient of k_i; PBPK, physiologically based pharmacokinetics; NP, nanoparticle; Br, brain; Ca, carcass; GI, gastrointestinal; LI, liver; KI, kidney.

system, 3) excretion and elimination rates are described as first-order processes, and 4) complete equilibrium in a chemical exists between blood and tissue phases. Almost all PBPK models can be described by mass balance equations.

Table 1 lists the detailed PBPK model equations and symbols. The model equations were constructed according to the mass transfer of zinc (Zn)-containing chemicals and the physiological properties of mice. The liver, GI tract, and
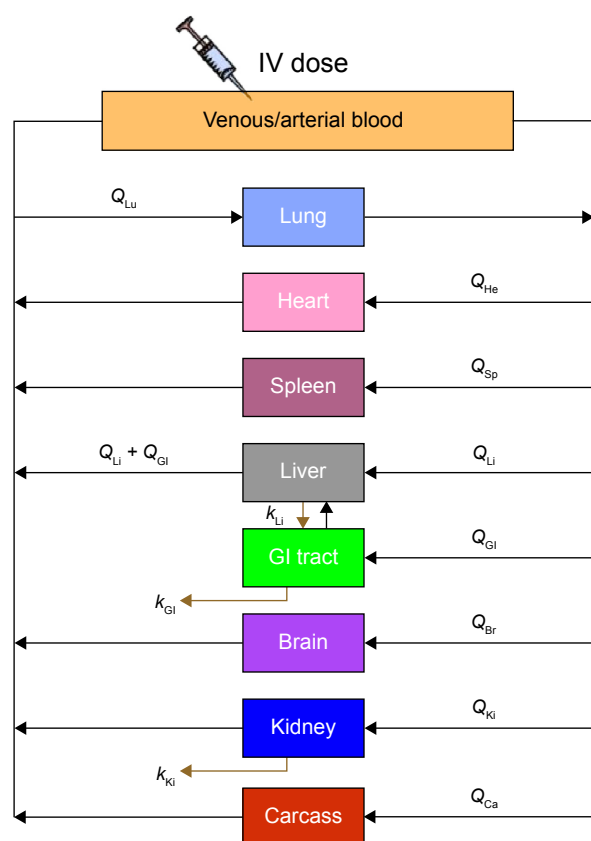
Figure 2 Constructed PBPK model describing the transportation of 10 nm and 71 nm ^{65}ZnO NPs and ^{65}Zn^{2+} and interactions between blood and tissues or organs.
Abbreviations: PBPK, physiologically based pharmacokinetic; NP, nanoparticle; IV, intravenous; GI, gastrointestinal; Q, blood flow to organ; k, excretion or elimination rate; Li, liver; Ki, kidney; Sp, spleen; Lu, lung; Br, brain; He, heart; Ca, carcass.

kidney are the major excreting and eliminating tissues for ^{65}ZnO NPs and ^{65}Zn(NO$_3$)$_2$.

Physiological parameters, including blood and tissue volumes, can be obtained from the experimental data. Exchange rates between tissue and blood compartments can be expressed as a fraction of cardiac output (Q_{Bl}, L·h^{-1}), in which cardiac output is scaled to body weight using the allometric equation,

$$Q_{Bl} = Q_C \, BW^{0.75} \qquad (1)$$

where Q_C is the cardiac output constant for a 1 kg mice and BW is the body weight (kg).[13] Organ volume constants (V_i) of mice were scaled to body weight based on a previous study.[7] Table 2 lists all physiological parameters used in PBPK modeling.

Parameterization and validation

To acquire the physicochemical parameters of 10 nm and 71 nm ^{65}ZnO NPs and ^{65}Zn(NO$_3$)$_2$, the time-dependent tissue partition coefficients (p_i) and excretion and elimination rates (k_i) were considered. The tissue partition coefficient can be estimated by the area under the curve of ^{65}Zn^{2+} or ^{65}ZnO NPs in tissues or blood. Monte Carlo simulation was performed using the calculated mean and standard deviation of the area under the curve of tissues and blood to obtain the distribution of tissue partition coefficients for blood and tissue samples with various

Table 1 Physiologically based pharmacokinetic model equations in mice

Compartments	Equations	Equation ID
Blood (C_{Bl}, µg·mL^{-1})	$\dfrac{dC_{Bl}}{dt} = \dfrac{1}{V_{Bl}}\left(\begin{array}{l} Q_{Lu}\cdot\dfrac{C_{Lu}}{p_{Lu}} + Q_{Sp}\cdot\dfrac{C_{Sp}}{p_{Sp}} + (Q_{Li}+Q_{GI})\cdot\dfrac{C_{Li}}{p_{Li}} \\ +Q_{He}\cdot\dfrac{C_{He}}{p_{He}} + Q_{Br}\cdot\dfrac{C_{Br}}{p_{Br}} + Q_{Ki}\cdot\dfrac{C_{Ki}}{p_{Ki}} + Q_{Ca}\cdot\dfrac{C_{Ca}}{p_{Ca}} \end{array}\right)$ $-\dfrac{C_{Bl}}{V_{Bl}}\left(Q_{Lu}+Q_{Sp}+Q_{Li}+Q_{He}+Q_{Br}+Q_{Ki}+Q_{Ca}+Q_{GI}\right)$	(A)
Lung (C_{Lu}, µg·g^{-1})	$\dfrac{dC_{Lu}}{dt} = \dfrac{Q_{Lu}}{V_{Lu}}\left(C_{Bl} - \dfrac{C_{Lu}}{p_{Lu}}\right)$	(B)
GI tract (C_{GI}, µg·g^{-1})	$\dfrac{dC_{GI}}{dt} = \dfrac{Q_{GI}}{V_{GI}}\left(C_{Bl} - \dfrac{C_{GI}}{p_{GI}}\right) + C_{Li}\cdot k_{Li}/p_{Li} - C_{GI}\cdot k_{GI}/p_{GI}$	(C)
Spleen (C_{Sp}, µg·g^{-1})	$\dfrac{dC_{Sp}}{dt} = \dfrac{Q_{Sp}}{V_{Sp}}\left(C_{Bl} - \dfrac{C_{Sp}}{p_{Sp}}\right)$	(D)
Liver (C_{Li}, µg·g^{-1})	$\dfrac{dC_{Li}}{dt} = \dfrac{1}{V_{Li}}\left(Q_{Li}\cdot C_{Bl} + Q_{GI}\cdot\dfrac{C_{GI}}{p_{GI}} - (Q_{Li}+Q_{GI})\cdot\dfrac{C_{Li}}{p_{Li}}\right) - C_{Li}\cdot k_{Li}/p_{Li}$	(E)

(Continued)

Table 1 (*Continued*)

Compartments	Equations	Equation ID
Heart (C, $\mu g \cdot g^{-1}$)	$\dfrac{dC_{He}}{dt} = \dfrac{Q_{He}}{V_{He}}\left(C_{Bl} - \dfrac{C_{He}}{p_{He}}\right)$	(F)
Brain (C_{Br}, $\mu g \cdot g^{-1}$)	$\dfrac{dC_{Br}}{dt} = \dfrac{Q_{Br}}{V_{Br}}\left(C_{Bl} - \dfrac{C_{Br}}{p_{Br}}\right)$	(G)
Kidney (C_{Ki}, $\mu g \cdot g^{-1}$)	$\dfrac{dC_{Ki}}{dt} = \dfrac{Q_{Ki}}{V_{Ki}}\left(C_{Bl} - \dfrac{C_{Ki}}{p_{Ki}}\right) - C_{Ki} \cdot k_{Ki}/p_{Ki}$	(H)
Carcass (C_{Ca}, $\mu g \cdot g^{-1}$)	$\dfrac{dC_{Ca}}{dt} = \dfrac{Q_{Ca}}{V_{Ca}}\left(C_{Bl} - \dfrac{C_{Ca}}{p_{Ca}}\right)$	(I)

Abbreviations: C, concentration; V, tissue volume; Q, Blood flow to organ; p, partition coefficient; k, excretion or elimination rate; Bl, blood; Li, liver; Ki, kidney; Sp, spleen; Lu, lung; Br, brain; He, heart; GI, gastrointestinal; Ca, carcass.

plausible combinations. The distributions were assumed to be lognormal to avoid negative values caused by high deviations. The individual variability of mice was also incorporated into the tissue partition coefficient estimates. The time-dependent partition coefficients for carcass and brain were sigmoidal, whereas a peak curve was observed for other tissues. Crystal Ball® software (Version 2000.2; Decisioneering Inc, Denver, CO, USA) was used for Monte Carlo simulation to obtain the 2.5 and 97.5 percentiles as 95% confidence intervals.

Table 2 Physiological parameters used in PBPK model for ^{65}ZnO NPs and ^{65}Zn(NO$_3$)$_2$ in mice

Symbol	Value	Description (unit)	Source
BW	0.032	Body weight (kg)	Estimated
Q_C	9.025	Cardiac output constant ($L \cdot h^{-1}$)	Davies and Morris[13]
Organ volume (as percentage of BW)			
V_{Bl}	0.060	Blood volume	Estimated
V_{Lu}	0.007	Lung volume	Estimated
V_{GI}	0.127	GI tract volume	Estimated
V_{Sp}	0.004	Spleen volume	Estimated
V_{Li}	0.059	Liver volume	Estimated
V_{He}	0.007	Heart volume	Estimated
V_{Br}	0.014	Brain volume	Estimated
V_{Ki}	0.016	Kidney volume	Estimated
V_{Ca}	0.706	Carcass volume	Estimated
Blood flow to organ (as percentage of cardiac output)			
Q_{Lu}	1	Lung blood flow	Brown et al[18]
Q_{GI}	0.188	GI tract blood flow	Davies and Morris[13]
Q_{Sp}	0.011	Spleen blood flow	Davies and Morris[13]
Q_{Li}	0.161	Liver blood flow	Davies and Morris[13]
Q_{He}	0.060	Heart blood flow	Brown et al[18]
Q_{Br}	0.030	Brain blood flow	Brown et al[18]
Q_{Ki}	0.091	Kidney blood flow	Brown et al[18]
Q_{Ca}	0.454	Carcass blood flow	Estimated

Abbreviations: PBPK, physiologically based pharmacokinetic; NP, nanoparticle; BW, body weight; GI, gastrointestinal; Q_c, cardiac output constant; V, tissue volume; Q, Blood flow to organ; Bl, blood; Li, liver; Ki, kidney; Sp, spleen; Lu, lung; Br, brain; He, heart; Ca, carcass.

A four-parameter Hill function can be used to describe the time-dependent partition coefficient of heart, brain, and carcass in ^{65}Zn(NO$_3$)$_2$ and that of brain and carcass in 10 nm and 70 nm ^{65}ZnO NPs in a sigmoid manner,

$$p_i(t) = p_{i,ini} + \frac{(p_{i,max} - p_{i,ini}) \cdot t^{n_{p_i}}}{Tp_{i,50}^{n_{p_i}} + t^{n_{p_i}}} \tag{2}$$

where $p_i(t)$ is the time-dependent partition coefficient ($-$), $p_{i,ini}$ is the initial partition coefficient ($-$), $p_{i,max}$ is the maximum partition coefficient ($-$), $Tp_{i,50}$ is the time constant at 50% maximum partition coefficient (hours), t is the time (hours), and n_{pi} is the Hill coefficient ($-$).

Typically, excretion or elimination rate constant estimates can be determined by a depuration process in a contaminated organism without ^{65}ZnO NP or ^{65}Zn(NO$_3$)$_2$ injection. Therefore, the kinetics of the depuration process,

$$C_i(t) = C_i(t=T)e^{-k_i t} \tag{3}$$

where $C_i(t)$ is the time-dependent ^{65}ZnO NP or ^{65}Zn(NO$_3$)$_2$ concentration in tissue i ($\mu g \cdot g^{-1}$), $C_i(t=T)$ is the concentration at time T (hours) when depuration begins, and k_i is the excretion or elimination rate constant (h^{-1}), can be used to estimate excretion or elimination rate constants. The results at the end of the experimental period showed that the accumulated Zn was substantially less than the initial administered dose. Thus, time-dependent maximum and half-maximum excretion or elimination rates can also markedly affect ^{65}ZnO NP or ^{65}Zn(NO$_3$)$_2$ accumulation.

Time-dependent excretion and elimination were considered to occur in ^{65}ZnO NP or ^{65}Zn(NO$_3$)$_2$ kinetic processes,

$$k_i(t) = k_{i,min} + \frac{(k_{i,max} - k_{i,min})}{\left(1 + \left(\frac{t}{Tk_{i,50}}\right)^{n_{k_i}}\right)} \quad (4)$$

where $k_{i,min}$ is the minimum excretion or elimination rate constant (h^{-1}), $k_{i,max}$ is the maximum excretion or elimination rate constant (h^{-1}), $Tk_{i,50}$ is the time constant at 50% maximum excretion or elimination rate (hours), and n_{k_i} is the Hill coefficient (−). TableCurve 2D (Version 5; AISN Software Inc, Mapleton, OR, USA) was used to fit the experimental data to obtain the optimally fitted statistical model. The generated coefficients of determination (r^2) can be used to examine the goodness of fit of selected nonlinear statistical models.

To investigate differences in size- and tissue-specific accumulation trends, mean residence times of ^{65}ZnO NPs and ^{65}Zn(NO$_3$)$_2$ in tissues were calculated. Mathematically, mean residence time can be defined as:

$$\bar{t_i} = \frac{\int_0^t t C_i(t) dt}{\int_0^t C_i(t) dt} \quad (5)$$

where $\bar{t_i}$ is the mean residence time (hours) and $C_i(t)$ is the tissue concentration profile ($\mu g \cdot g^{-1}$).[14]

The Berkeley Madonna: Modeling and Analysis of Dynamic Systems (Version 8.3.9; University of California, Berkley, CA, USA) was used to perform all PBPK simulations for ^{65}ZnO NPs and ^{65}Zn(NO$_3$)$_2$ in mice. To assess the performance of model predictability, the mean absolute percentage error (MAPE) was calculated as:[15,16]

$$MAPE = \frac{1}{N} \sum_{n=1}^{N} \frac{|C_{o,n} - C_{m,n}|}{C_{o,n}} \times 100\%, \quad (6)$$

where N denotes the number of observations, $C_{o,n}$ is the observed biodistribution data from blood and each tissue of ^{65}ZnO NPs and ^{65}Zn(NO$_3$)$_2$, and $C_{m,n}$ is the modeled result corresponding to blood- and tissue-specific data point n. Further calibration might be required to obtain the optimal fit of pharmacokinetics to experimental data. To perform further calibration of the experimental data, the estimated tissue-specific excretion or elimination rates and partition coefficients would be adjusted based on our study hypothesis and the characteristics of ^{65}ZnO NPs and ^{65}Zn(NO$_3$)$_2$ to reduce the MAPE values.

Sensitivity analysis

A sensitivity analysis was performed to identify the influence of critical variables in the algorithm on tissue accumulation.

To test sensitivity, the partition coefficients and excretion and elimination rates were increased by 10% to iterate the model simulation and to identify significant changes in the modeled accumulation distribution. The sensitivity ratios were calculated as:

$$SR = \frac{\Delta C / C_o}{\Delta x / x_o}, \quad (7)$$

where ΔC is the difference between the resulting and original (Y_o) predicted concentration values, and Δx is the difference between the resulting and initial (x_o) parameter values.

Results

Particle size-dependent physicochemical parameters

Our results indicated that the calculated tissue partition coefficients of 10 nm ^{65}ZnO NPs were greater than those of 71 nm ^{65}ZnO NPs and ^{65}Zn(NO$_3$)$_2$, except for the partition coefficients of 71 nm ^{65}ZnO NPs in the liver and kidney at 672 hours, GI tract at 24–672 hours, and carcass at 1 hour and 24–672 hours. Tables S1–S3 list the detailed time-dependent partition coefficients of 10 nm and 71 nm ^{65}ZnO NPs and ^{65}Zn(NO$_3$)$_2$. The increases in the partition coefficients of brain and carcass were time-dependent. The four-parameter Hill function in Equation 2 was optimally fitted to the partition coefficient of brain and carcass over time (r^2=0.97–0.99), and Hill coefficients were significant (>1) for both. Table 3 shows the estimates of the Hill parameters for brain and carcass partition coefficients.

Table S4 lists the estimated excretion or elimination rate constants of ^{65}ZnO NPs and ^{65}Zn(NO$_3$)$_2$. The estimated time-dependent excretion or elimination rates for 10 nm and 71 nm ^{65}ZnO NPs and ^{65}Zn(NO$_3$)$_2$ marginally decreased during the 28-day experimental period. Furthermore, a significant decreasing trend of excretion or elimination rate following the order ^{65}Zn(NO$_3$)$_2$, 71 nm ^{65}ZnO NPs, and 10 nm ^{65}ZnO NPs were observed in kidneys and GI tract and not in the liver (Table S4).

Simulation and model validation

Figures 3 and 4 show comparisons between the results from PBPK model simulation (solid line, without calibration; dashed line, with calibration, after 7 days of exposure) and the experimental data on tissue and blood concentrations of 10 nm and 71 nm ^{65}ZnO NPs and ^{65}Zn(NO$_3$)$_2$. To perform PBPK simulation, we considered the time-dependent excretion or elimination rates and partition coefficients of 10 nm and 71 nm ^{65}ZnO NPs and ^{65}Zn(NO$_3$)$_2$.

Table 3 Physicochemical parameters used in PBPK model for ^{65}ZnO NPs and ^{65}Zn(NO$_3$)$_2$ in mice

Parameter	10 nm ^{65}ZnO NPs[a]					71 nm ^{65}ZnO NPs[a]					^{65}Zn(NO$_3$)$_2$				
	X_{ini}	X_{max}	TX_{50}	X_n	r^2	X_{ini}	X_{max}	TX_{50}	X_n	r^2	X_{ini}	X_{max}	TX_{50}	X_n	r^2
Partition coefficient (−)															
p_{Li}	8.1[b]					6.28					2.1				
p_{Ki}	7.11					3.52					2.1				
p_{Sp}	6					3.7,[c] 1.44[d]					1.3				
p_{Lu}	64,[e] 6.33[f]					3.78					0.95				
p_{He}	2.55					1.22					0.24	0.93	3.31	2.96	0.99
p_{GI}	4.4					2.70					1.7				
p_{Br}	0.33	2.87	82.532	1.014	0.97	0.002	1.969	61.970	0.711	0.98	0.024	0.748	55.614	0.929	0.99
p_{Ca}	0.77	2.67	8.505	1.007	0.98	0.0002	5.463	103.700	0.483	0.98	0.085	1.157	22.680	0.567	0.99
Excretion/ elimination rate (h^{-1})															
k_{GI}	0.017	0.034	19.639	1.850	0.99	0.079					0.07				
k_{Li}	0.019	0.031	41.822	3.246	0.99	0.023					0.04				
k_{Ki}	0.010	0.032	12.954	1.465	0.99	0.128					0.02	0.07	16.4	1.90	0.99

Notes: Time-dependent parameters including partition coefficients p_{He} of ^{65}Zn(NO$_3$)$_2$, p_{Br}, and p_{Ca}, as well as excretion/elimination rates of 10 nm ^{65}ZnO NPs (k_{GI}, k_{Li}, and k_{Ki}) and k_{Ki} of ^{65}Zn(NO$_3$)$_2$ were estimated by fitting with Hill equation. [a]Physicochemical parameters are only fitted to use on early phase (first 7 days). [b]Constant parameter used in PBPK model. [c]Constant parameter used in PBPK model during first 3 days. [d]Constant parameter used in PBPK model during days 3–7. [e]Constant parameter used in PBPK model during first 7 hours. [f]Constant parameter used in PBPK model during hour 7 to day 7. Blank spaces in the table indicate that these partition coefficients (p_{Li}, p_{Ki}, p_{Sp}, p_{Lu}, p_{He}, p_{GI}) were constant values (X_{ini}), not time-dependent and, therefore, no related estimated values of X_{max}, TX_{50}, X_n and r^2 for these partition coefficients.
Abbreviations: −, no units; PBPK, physiologically based pharmacokinetic; NP, nanoparticle; p, partition coefficient; k, excretion or elimination rate; Li, liver; Ki, kidney; Sp, spleen; Lu, lung; Br, brain; He, heart; GI, gastrointestinal; Ca, carcass.

Specifically, the concentration of 10 nm ^{65}ZnO NPs in the lung showed a higher accumulative capacity than those of 71 nm ^{65}ZnO NPs and ^{65}Zn(NO$_3$)$_2$ for the first 7 hours (Figure 3). Moreover, the concentration of 71 nm ^{65}ZnO NPs decreased substantially to almost zero from days 3 to 7 in the spleen. Therefore, we used optimized partition coefficients (listed in Table 3) to simulate and describe ^{65}ZnO NPs concentration profiles over time in the lung and spleen (Figure 3A–F).

The majority of the experimental concentration profiles of ^{65}ZnO NPs and ^{65}Zn(NO$_3$)$_2$ in the target tissues of mice rapidly increased within a few hours of intravenous injection and decreased thereafter (Figures 3A–R and 4), whereas concentrations profiles in the brain and carcass increased and then slightly decreased during the 7-day period (Figure 3S–X). The time-dependent increasing functions of the partition coefficients might thus be suitable to describe the biodistributions of ^{65}ZnO NPs and ^{65}Zn(NO$_3$)$_2$ in mice brain and carcass (Table 3).

During the late phase (days 7–28), we observed that tissue concentration markedly decreased and that our simulation of ^{65}ZnO NPs barely fit the experimental data. Yet, the simulation of ^{65}Zn(NO)$_3$ was well fitted with the experimental data. Therefore, it is likely that ^{65}ZnO NPs gradually decompose into zinc ion after 7 days. Indeed, similar results were also observed in a previous study.[17] We proposed that the ^{65}ZnO NPs might decompose after day 7, resulting in a markedly decreasing trend on day 28. For that, we replaced the partition coefficients and excretion or elimination rates of 10 nm and 71 nm ^{65}ZnO NPs after day 7 with those estimated from ^{65}Zn(NO$_3$)$_2$ experimental data. All partition coefficients used for calibration are listed in Table 4.

Overall, our results indicated that the PBPK simulations with calibration reasonably agreed with the experimentally determined values of the time-dependent ^{65}ZnO NP and ^{65}Zn(NO$_3$)$_2$ concentrations (MAPE <50%) (Figure 5). Notably, 10 nm ^{65}ZnO NPs of the heart and brain and 71 nm ^{65}ZnO NPs of the liver and carcass provided good predictions (10%≤ MAPE <20%). The PBPK simulation outcome for ^{65}Zn(NO$_3$)$_2$ concentration in the kidney provided an excellent prediction (MAPE <10%).

Mean residence time estimation and sensitivity analysis

We used the experimental accumulation data obtained using Equation 5 to estimate the mean residence times of ^{65}ZnO NPs and ^{65}Zn(NO$_3$)$_2$ in each tissue. As shown in Figure 6A, the mean residence times of the majority of tissues ranged from 7 days to 14 days. Generally, the mean residence time of 10 nm ^{65}ZnO NPs was longer than those of ^{65}Zn(NO$_3$)$_2$ and 71 nm ^{65}ZnO NPs (Figure 6B). These results indicated that 10 nm ^{65}ZnO NPs in the blood, brain, heart, and carcass and 71 nm ^{65}ZnO NPs and ^{65}Zn(NO$_3$)$_2$ in the brain and carcass had mean residence times close to the highest outliers
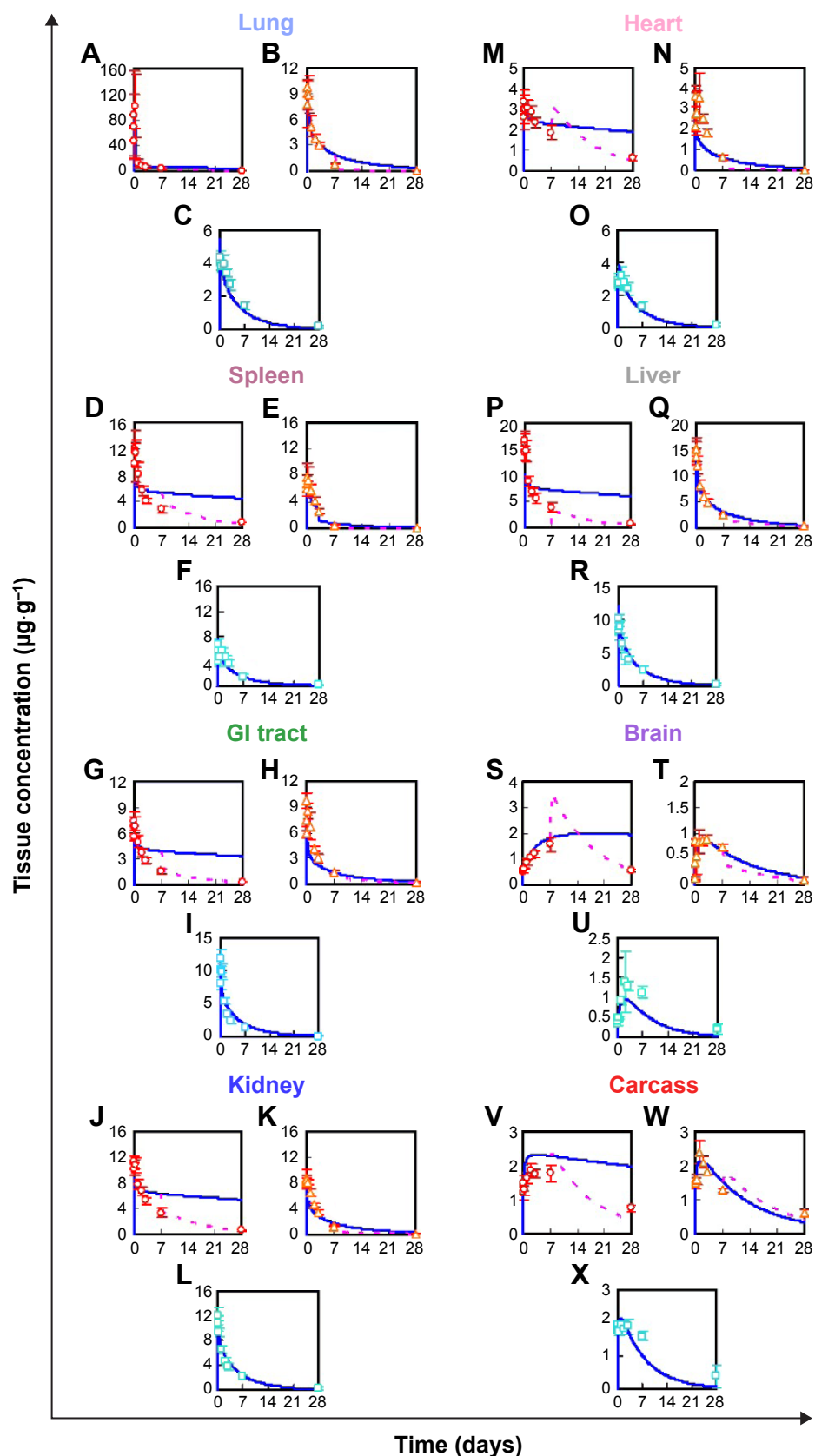
Figure 3 Comparisons between PBPK model simulations and pharmacokinetics in mice lung (**A–C**), spleen (**D–F**), GI tract (**G–I**), kidney (**J–L**), heart (**M–O**), liver (**P–R**), brain (**S–U**), and carcass (**V–X**) after intravenous injection of 10 nm (circle) and 71 nm (triangle) ^{65}ZnO NPs and ^{65}Zn(NO$_3$)$_2$ (square).
Note: Solid and dashed lines represent simulations without and with calibration, respectively, before and after 7-day exposure.
Abbreviations: PBPK, physiologically based pharmacokinetic; NP, nanoparticle; GI, gastrointestinal.
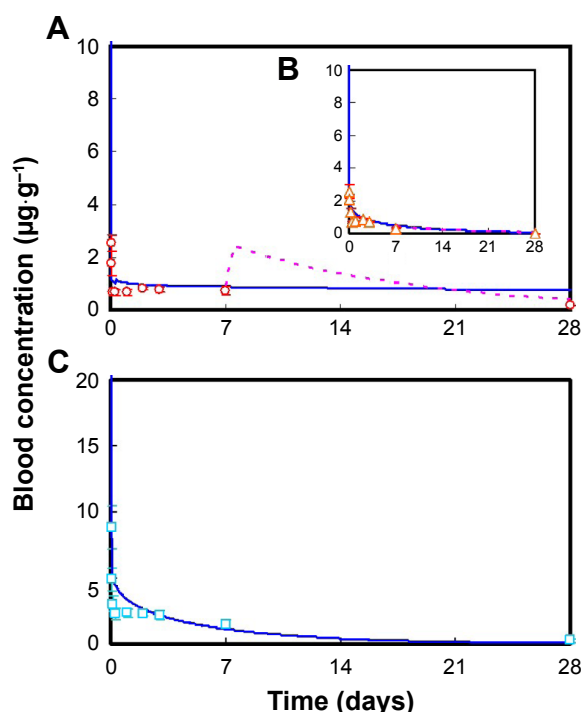
Figure 4 Comparisons between PBPK model simulations and pharmacokinetics of mice in blood after intravenous injection of (**A**) 10 nm and (**B**) 71 nm ^{65}ZnO NPs, and (**C**) ^{65}Zn(NO$_3$)$_2$.
Notes: Solid and dashed lines represent simulations without and with calibration, respectively. Circles, triangles, and squares represent blood concentration data of 10 nm, and 71 nm ^{65}ZnO NP, and ^{65}Zn(NO$_3$)$_2$, respectively.
Abbreviations: PBPK, physiologically based pharmacokinetic; NP, nanoparticle.

of 14 days, whereas 71 nm ^{65}ZnO NPs in the spleen had the lowest mean residence time of 4.55 days (95% confidence interval: 1.14–2.07).

Figure 7 shows the critical variables in our sensitivity analyses for tissue concentrations during the 7-day period. The sensitivity analyses indicated that ^{65}Zn(NO$_3$)$_2$ tissue concentrations were most sensitive to the increased

Table 4 Physicochemical parameters used in PBPK model for ^{65}ZnO NPs in mice after day 7

Parameter	10 nm ^{65}ZnO NPs	71 nm ^{65}ZnO NPs
Partition coefficient (−)		
p_{Li}	1.32	3.53
p_{Ki}	1.42	0.91
p_{Sp}	1.54	0.26
p_{Lu}	1.25	0.34
p_{He}	1.25	0.20
p_{GI}	0.63	1.63
p_{Br}	1.42	0.93
p_{Ca}	0.96	4.45
Excretion/elimination rate (h^{-1})		
k_{GI}	0.0343	0.0788
k_{Li}	0.0192	0.0229
k_{Ki}	0.0319	0.1277

Abbreviations: PBPK, physiologically based pharmacokinetic; NP, nanoparticle; Li, liver; Ki, kidney; Sp, spleen; Lu, lung; Br, brain; He, heart; GI, gastrointestinal; Ca, carcass.
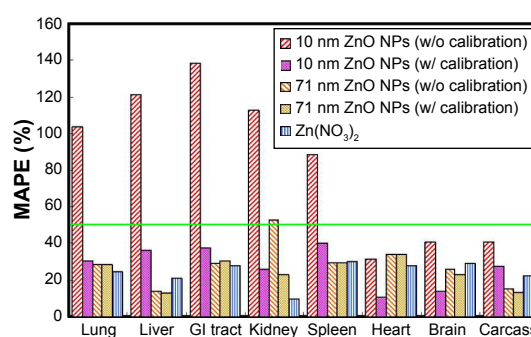

Figure 5 MAPE estimates showing the performances of model predictability of 10 nm and 71 nm ^{65}ZnO NPs and ^{65}Zn(NO$_3$)$_2$, with and without calibration.
Note: The horizontal line indicates reasonable prediction with MAPE <50%.
Abbreviations: MAPE, mean absolute percentage error; NP, nanoparticle; w/, with; w/o, without; GI, gastrointestinal.

excretion or elimination rate of the liver (k_{Li}, sensitive coefficient: 0.46) and that the partition coefficient of the lung (p_{Lu}) presented the most sensitive coefficient of 0.54 in 10 nm ^{65}ZnO NPs. However, parameters that increased in correspondence with a decrease in tissue concentration included the excretion or elimination rates of the GI tract and kidney for all chemicals, the partition coefficients of the GI tract (−0.06) and carcass (−0.32) for 10 nm ^{65}ZnO NPs, and the partition coefficients of the carcass (−0.14) for 71 nm ^{65}ZnO NPs.

Discussion

ZnO NP has been proposed to gradually decompose into zinc ion in the biological system. However, our data showed that the tissue kinetics of ^{65}ZnO NP were still different from those of zinc ion in mice. By comparing the PBPK parameters of ^{65}ZnO NP and ^{65}Zn^{2+}, we are able to propose that majority of ^{65}ZnO NP in tissues might decompose after day 7. And incorporating the parameters of zinc ion into ^{65}ZnO NP model after day 7 would improve the simulation. Our study shows that it is possible to construct a PBPK model for slowly decomposed NPs, by comparing the kinetics of NPs and soluble elements.

Critical parameters and associated effects of PBPK model

Our ^{65}ZnO NP PBPK model for ^{65}ZnO NPs fitted well with the accumulation of various size ^{65}ZnO NPs in mice tissues. In a PBPK model, the partition coefficient is the key parameter affecting accumulation levels in tissues.[18] Although it is often assumed that partitioning between tissues and blood reaches equilibrium after 24 hours, increasing evidence suggests that equilibrium for NPs in specific tissues is reached after several days to several months and that the concentrations in these
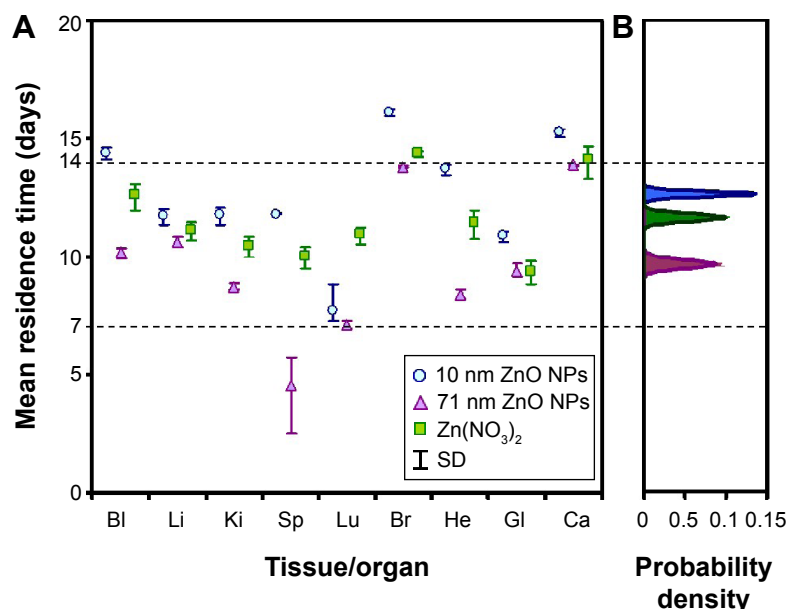
Figure 6 Tissue-specific mean residence times and probability density of 10 nm and 71 nm ^{65}ZnO NPs and ^{65}Zn(NO$_3$)$_2$ accumulations.
Notes: (**A**) Tissue-specific mean residence times of 10 nm and 71 nm ^{65}ZnO NPs and ^{65}Zn(NO$_3$)$_2$ (range: 7–14 days) and (**B**) probability density distributions of mean residence times of 10 nm (blue) and 71 nm (purple) ^{65}ZnO NPs and ^{65}Zn(NO$_3$)$_2$ (green).
Abbreviations: NP, nanoparticle; SD, standard deviation; Bl, blood; Li, liver; Ki, kidney; Sp, spleen; Lu, lung; Br, brain; He, heart; GI, gastrointestinal; Ca, carcass.

organs can increase several fold with increasing duration of exposure.[19–23] Thus, the constant partition coefficients estimated from the steady-state condition might not be able to assess the biodistributions of ^{65}ZnO NPs and ^{65}Zn(NO$_3$)$_2$ in target tissues.
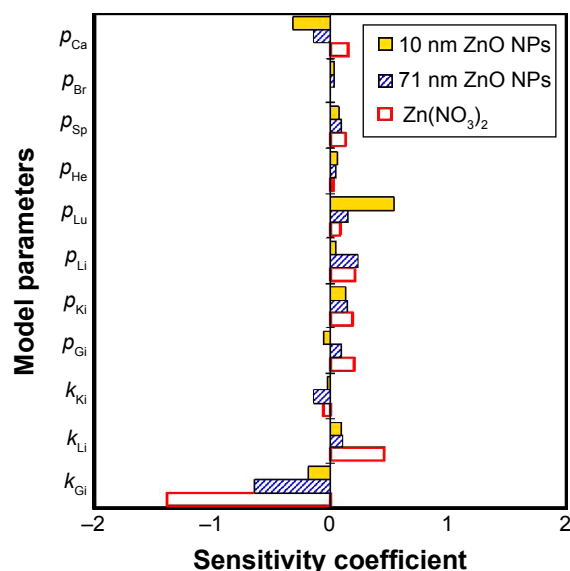

Figure 7 Sensitivity analysis of partition coefficients and excretion or elimination rates in the mice PBPK model.
Note: Right and left sides indicate the effects of increases in parameters on tissue concentration.
Abbreviations: PBPK, physiologically based pharmacokinetic; NP, nanoparticle; p, partition coefficient; k, excretion or elimination rate; Li, liver; Ki, kidney; Sp, spleen; Lu, lung; Br, brain; He, heart; GI, gastrointestinal; Ca, carcass.

We observed that the partition coefficient in the lung (p_{Lu}) was particularly high for 10 nm ^{65}ZnO NPs and that p_{Lu} was the most sensitive parameter of the biodistribution of 10 nm ^{65}ZnO NPs. This result might have been caused by the lung being the first organ with a reticuloendothelial system in contact with ^{65}ZnO NPs following intravenous injection. NPs are readily uptaken by phagocytic cells in the reticuloendothelial system. It is thus likely that alveolar macrophages in the lung would capture 10 nm ^{65}ZnO NPs before translocating to the lymphatic tissue, and then trapped ^{65}ZnO NPs would be redistributed to other tissues over a longer duration. Our results support those hypotheses.[24,25] However, at later time points, ^{65}ZnO NPs failed to accumulate in the lung and its partition coefficients decreased, suggesting that this mechanism in the lung might not be crucial in long-term biodistribution.

Potential mechanisms for the biodistribution of NPs

The potential mechanisms for the biodistribution of NPs are complicated. Several factors such as interactions with biological barriers and NP properties (composition, size, core properties, and surface modifications) have been shown to significantly influence the biodistribution and blood circulation half-life of circulating NPs. A study indicated that partition coefficients of tissues or blood might be influenced by factors including blood flow and the turnover rate of each tissue, tissue affinity, and lipid composition.[26] An increased time-dependent partition coefficient in the liver in mice exposed
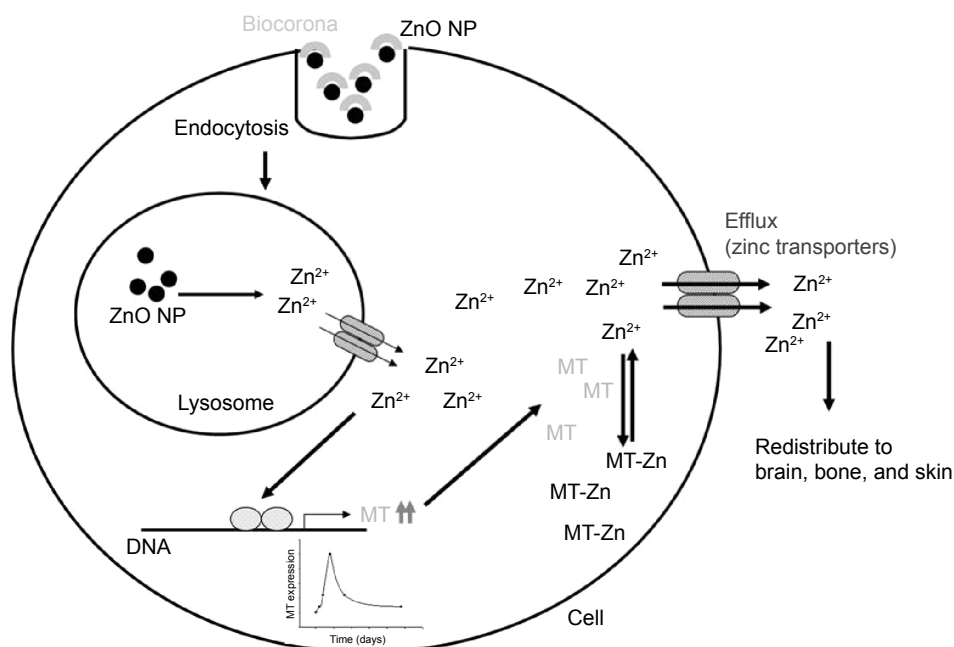
Figure 8 The proposed mechanisms for time-dependent partition coefficients in tissues.
Abbreviation: NP, nanoparticle.

to polychlorinated biphenyls was identified.[27] ZnO NPs might be persistent in the approximately neutral surfactant fluid or cytosol, yet it is rapidly converted to Zn^{2+} when ZnO NPs internalized into the acid environment of the lysosome.[17] From our previous studies and in vitro experiments, we proposed that ZnO NPs would decompose, release Zn^{2+}, and upregulate MT protein after endocytosis (Figure 8). Sadhu and Gedamu reported that the upregulation of MT decreased dynamically with time after exposure to Zn.[28] MT binds to intracellular Zn^{2+} and increases their accumulation in cells (Figure 8). When MT protein decreases at later time points, Zn^{2+} ions are pumped out of the cells by the Zn transporter, reenter the circulation, and are subsequently stored in muscle and bone (referred to as carcass in this study).[29,30] Therefore, the tissue partition coefficients of ZnO NPs might change time-dependently. Indeed, our results showed that the partition coefficients of ZnO NPs are dependent on time after exposure and might be affected by the decomposition of ZnO NPs (Figure 8). Also, the results have a good prediction when we replaced the partition coefficients and excretion or elimination rates of 10 nm and 71 nm ZnO NPs with that of Zn^{2+} after day 7 exposure.

Furthermore, NPs are reportedly readily uptaken by phagocytic cells in the liver, spleen, lung, and kidneys.[31] Therefore, ZnO NPs quickly distribute to these organs within 24 hours of exposure. Proteins associated with the surfaces of NPs are recognized by macrophages and might modulate the translocation and redistribution of NPs from blood by

organs with an reticuloendothelial system.[32] In addition, the uptake and internalization of NPs in the brain might be facilitated by the formation of a biocorona, with plasma proteins on the surface of NPs, which allows for the crossing of the brain–blood barrier.[33–35] Our data indicated that the relationship between time and partition coefficients in the brain and carcass differed from those in other tissues. Considering the unique biodistribution characteristics of ZnO NPs and Zn^{2+}, we used the Hill equation to describe partitioning between blood and tissues in a time-dependent manner. The time-dependent partition coefficients fitted well with the measurement data and enabled the construction of our PBPK model for ZnO NPs.

Implications

We observed that the partition coefficients of the brain (p_{Br}) and carcass (p_{Ca}) increased time-dependently. This indicates that irrespective of phase and size, ZnO NPs and $Zn(NO_3)_2$ preferentially redistribute to the brain and carcass at later time points after exposure. With high partition coefficient, the 10 nm ZnO NPs tend to redistribute and accumulate in the brain tissue. Although p_{Br} and p_{Ca} were relatively low following a single dose of the Zn compounds, multiple dosing for a long duration could potentially increase the accumulation of chemicals in the brain and carcass. Zn^{2+} ions are abundant in the brain and play crucial roles in learning and memory.[36] However, Zn overdose can cause spatial reference memory deficit in animals.[37]

It has been identified that ZnO NPs have the potential ability to damage and kill neural stem cells in mice.[38] Therefore, in future research, the cumulative and hazardous properties of ZnO NPs in the brain should be considered in long-term health assessments of brain damage and memory deficit.

The biodistribution of NPs is highly influenced by the cellular uptake of NPs through phagocytosis by the mononuclear phagocytic system. NPs can accumulate in phagocytic cells of specific organs including the liver, spleen, lung, kidney, and brain or redistribute to the lymphatic fluid. According to previous study, phagocytizing cells rapidly capture NPs until their saturation, constitute a major reservoir in richly perfused organs, including the spleen, liver, bone marrow, lungs, heart, and kidneys, and store 83% NPs in these organs 120 hours after injection.[39] To more comprehensively understand the role of the mononuclear phagocytic system in the biodistribution of NPs, we will include mononuclear phagocytic system subcompartments in these organs when we construct PBPK models for NPs in future studies.

A report investigated and compared ZnO NP and zinc chloride contents in the blood and observed that although ZnO NPs partly dissolve in gastric conditions (13%–14%), particles administered in various states produce different biodistribution profiles.[40] Although studies have demonstrated that ZnO NPs can dissolve in tissues and release Zn^{2+} within hours, the metabolic mechanisms leading to the various biodistribution profiles of NPs and ions remain unclear and warrant further investigation.[1,40] Given that the exposure doses and excretion or elimination rates of each tissue are known, a PBPK model suitable for transfer within various exposure routes (intravenous, inhalation, and oral) could be constructed.[41,42]

Conclusion

Despite certain data limitations, this study estimated and identified critical parameters influencing PBPK modeling in certain organs and tissues by using real-time mice exposure experiments. By considering the time-dependent partition coefficients and decomposition of ^{65}ZnO NPs into $^{65}Zn^{2+}$ after day 7, we increased the predictability of the PBPK model for exposure experimental data. The general patterns of bioaccumulation and biodistribution of ^{65}ZnO NPs and $^{65}Zn(NO_3)_2$ in mice were serviceably accurate.

In general, the tissue partition coefficients of ^{65}ZnO NPs were greater than those of $^{65}Zn(NO_3)_2$, particularly the partition coefficient of 10 nm ^{65}ZnO NPs in the lung. Sensitivity analysis revealed that 71 nm ^{65}ZnO NPs and $^{65}Zn(NO_3)_2$ were sensitive to excretion or elimination rates in the liver

and GI tract. We suggest caution against exposure to ZnO NPs <10 nm because they tend to accumulate in the body for a relatively longer duration than 71 nm ^{65}ZnO NPs and $^{65}Zn(NO_3)_2$ do. Although the partition coefficient of the brain was relatively low, it time-dependently increased for ^{65}ZnO NPs and $^{65}Zn(NO_3)_2$. Hazardous exposure risk for the brain must thus be carefully considered. In this study, we established a potentially predictive dynamic model for NPs, which we will investigate more comprehensively in future studies.

Author contributions

All authors contributed toward data analysis, drafting and critically revising the paper, and agree to be accountable for all aspects of the work.

Disclosure

The authors report no conflicts of interest in this work.

References

1. Vandebriel RJ, De Jong WH. A review of mammalian toxicity of ZnO nanoparticles. *Nanotechnol Sci Appl*. 2012;5:61–71.
2. Adamcakova-Dodd A, Stebounova LV, Kim JS, et al. Toxicity assessment of zinc oxide nanoparticles using sub-acute and sub-chronic murine inhalation models. *Part Fibre Toxicol*. 2014;11:1–15.
3. Chuang HC, Juan HT, Chang CN, et al. Cardiopulmonary toxicity of pulmonary exposure to occupationally relevant zinc oxide nanoparticles. *Nanotoxicology*. 2014;8:593–604.
4. Akhtar MJ, Ahamed M, Kumar S, Khan MM, Ahmad J, Alrokayan SA. Zinc oxide nanoparticles selectively induce apoptosis in human cancer cells through reactive oxygen species. *Int J Nanomedicine*. 2012;7: 845–857.
5. Cao Z, Zhang Z, Wang F, Wang G. Synthesis and UV shielding properties of zinc oxide ultrafine particles modified with silica and trimethyl siloxane. *Colloids Surf A Physicochem Eng Asp*. 2009;340:161–167.
6. Rasmussen JW, Martinez E, Louka P, Wingett DG. Zinc oxide nanoparticles for selective destruction of tumor cells and potential for drug delivery applications. *Expert Opin Drug Deliv*. 2010;7:1062–1077.
7. Yeh TK, Chen JK, Lin CH, et al. Kinetics and tissue distribution of neutron-activated zinc oxide nanoparticles and zinc nitrate in mice: effects of size and particulate nature. *Nanotechnology*. 2012;23:085102.

8. Krishnan K, Peyret T. Physiologically based toxicokinetic (PBTK) modeling in ecotoxicology. In: Devillers J, editor. *Ecotoxicology Modeling*. New York: Springer; 2009:145–175.

9. Peters SA. *Physiologically-Based Pharmacokinetic (PBPK) Modeling and Simulations*. New Jersey: John Wiley & Sons, Inc; 2012.

10. Zhou JG, Zhao FY, Wang YL, Zhang Y, Yang L. Size-controlled synthesis of ZnO nanoparticles and their photoluminescence properties. *J Lumin*. 2007;122:195–197.

11. Talam S, Karumuri SR, Gunnam N. Synthesis, characterization, and spectroscopic properties of ZnO nanoparticles. *ISRN Nanotechnol*. 2012; 2012:372505.

12. Uysala I, Severcana F, Evisa Z. Characterization by Fourier transform infrared spectroscopy of hydroxyapatite co-droped with zinc and flouoride. *Ceram Int*. 2013;39:7727–7733.

13. Davies B, Morris T. Physiological parameters in laboratory animals and humans. *Pharm Res*. 1993;10:1093–1095.

14. Cheng HY, Jusko WJ. Mean residence time concepts for pharmacokinetic systems with nonlinear drug elimination described by the Michaelis-Menten equation. *Pharm Res*. 1988;5:156–164.

15. Rayer S. Population forecast accuracy: does the choice of summary measure of error matter? *Popul Res Policy Rev*. 2007;26:163–184.

16. Wilson T. The forecast accuracy of Australian bureau of statistics national population projections. *J Popul Res*. 2007;24:91–117.

17. Cho WS, Duffin R, Howie SE, et al. Progressive severe lung injury by zinc oxide nanoparticles; the role of Zn^{2+} dissolution inside lysosomes. *Part Fibre Toxicol*. 2011;8:1–27.

18. Brown RP, Delp MD, Lindstedt SL, Rhomberg LR, Beliles RP. Physiological parameter values for physiologically based pharmacokinetic models. *Toxicol Ind Health*. 1997;13:407–484.

19. Wang J, Liu Y, Jiao F, et al. Time-dependent translocation and potential impairment on central nervous system by intranasally instilled TiO_2 nanoparticles. *Toxicology*. 2008;254:82–90.

20. Cho M, Cho WS, Choi M, et al. The impact of size on tissue distribution and elimination by single intravenous injection of silica nanoparticles. *Toxicol Lett*. 2009;189:177–183.

21. Lankveld DP, Oomen AG, Krystek P, et al. The kinetics of the tissue distribution of silver nanoparticles of different sizes. *Biomaterials*. 2010;31:8350–8361.

22. Wenger Y, Schneider RJ 2nd, Reddy GR, Kopelman R, Jolliet O, Philbert MA. Tissue distribution and pharmacokinetics of stable polyacrylamide nanoparticles following intravenous injection in the rat. *Toxicol Appl Pharmacol*. 2011;251:181–190.

23. Dziendzikowska K, Gromadzka-Ostrowska J, Lankoff A, et al. Time-dependent biodistribution and excretion of silver nanoparticles in male Wistar rats. *J Appl Toxicol*. 2012;32:920–928.

24. Park K, Park EJ, Chun IK, et al. Bioavailability and toxicokinetics of citrate-coated silver nanoparticles in rats. *Arch Pharm Res*. 2011;34: 153–158.

25. Takenaka S, Karg E, Roth C, et al. Pulmonary and systemaic distribution of inhaled ultrafine silver particles in rats. *Environ Health Perspect*. 2001;109(suppl 4):547–551.

26. Weijs L, Yang RS, Covaci A, Das K, Blust R. Physiologically based pharmacokinetic (PBPK) models for lifetime exposure to PCB 153 in male and female harbor porpoises (*Phocoena phocoena*): model development and evaluation. *Environ Sci Technol*. 2010;44:7023–7030.

27. Lee SK, Ou YC, Yang RSH. Comparison of pharmacokinetic interactions and physiologically based pharmacokinetic modeling of PCB 153 and PCB 126 in non-pregnant mice, lactating mice, and suckling pups. *Toxicol Sci*. 2002;65:26–34.

28. Sadhu C, Gedamu L. Metal-specific posttranscriptional control of human metallothionein genes. *Mol Cell Biol*. 1989;9:5738–5741.

29. Lichten LA, Cousins RJ. Mammalian zinc transporters: nutritional and physiologic regulation. *Annu Rev Nutr*. 2009;29:153–176.

30. King JC, Shames DM, Woodhouse LR. Zinc homeostasis in humans. *J Nutr*. 2000;130:1360S–1366S.

31. Moghimi SM, Hunter AC, Murray JC. Long-circulating and target-specific nanoparticles: theory to practice. *Pharmacol Rev*. 2001;53:283–318.

32. Li SD, Huang L. Nanoparticles evading the reticuloendothelial system: role of the supported bilayer. *Biochim Biophys Acta*. 2009;1788: 2259–2266.

33. Lundqvist M, Stigler J, Elia G, Lynch I, Cedervall T, Dawson KA. Nanoparticle size and surface properties determine the protein corona with possible implications for biological impacts. *Proc Natl Acad Sci U S A*. 2008;105:14265–14270.

34. Nel AE, Mädler L, Velegol D, et al. Understanding biophysicochemical interactions at the nano-bio interface. *Nat Mater*. 2009;8:543–557.

35. Wiley DT, Webster P, Gale A, Davis ME. Transcytosis and brain uptake of transferrin-containing nanoparticles by tuning avidity to transferrin receptor. *Proc Natl Acad Sci U S A*. 2013;110:8662–8667.

36. Frederickson CJ, Koh JY, Bush AI. The neurobiology of zinc in health and disease. *Nat Rev Neurosci*. 2005;6:449–462.

37. Flinn JM, Hunter D, Linkous DH, et al. Enhanced zinc consumption causes memory deficits and increased brain levels of zinc. *Physiol Behav*. 2005;83:793–803.

38. Deng X, Luan Q, Chen W, et al. Nanosized zinc oxide particles induce neural stem cell apoptosis. *Nanotechnology*. 2009;20:115101.

39. Li D, Johanson G, Emond C, Carlander U, Philbert M, Jolliet O. Physiologically based pharmacokinetic modeling of polyethylene glycol-coated polyacrylamide nanoparticles in rats. *Nanotoxicology*. 2014;8(S1):128–137.

40. Paek HJ, Lee YJ, Chung HE, et al. Modulation of the pharmacokinetics of zinc oxide nanoparticles and their fates in vivo. *Nanoscale*. 2013;5: 11416–11427.

41. Bachler G, von Goetz N, Hungerbühler K. A physiologically based pharmacokinetic model for ionic silver and silver nanoparticles. *Int J Nanomedicine*. 2013;8:3365–3382.

42. Li M, Reineke J. Mathematical modelling of nanoparticle biodistribution: extrapolation among intravenous, oral and pulmonary administration routes. *Int J Nano Biomater*. 2011;3:222–238.
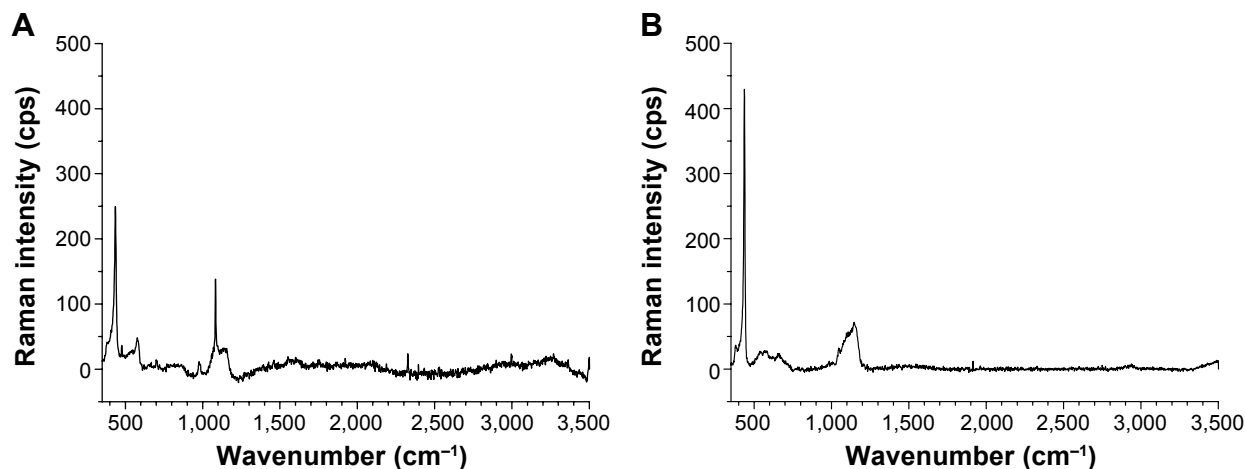
Supplementary materials

A

B

Figure S1 Raman spectra of ZnO NPs.
Notes: Raman spectra of (**A**) 10 nm and (**B**) 71 nm ZnO NPs.
Abbreviation: NP, nanoparticle.
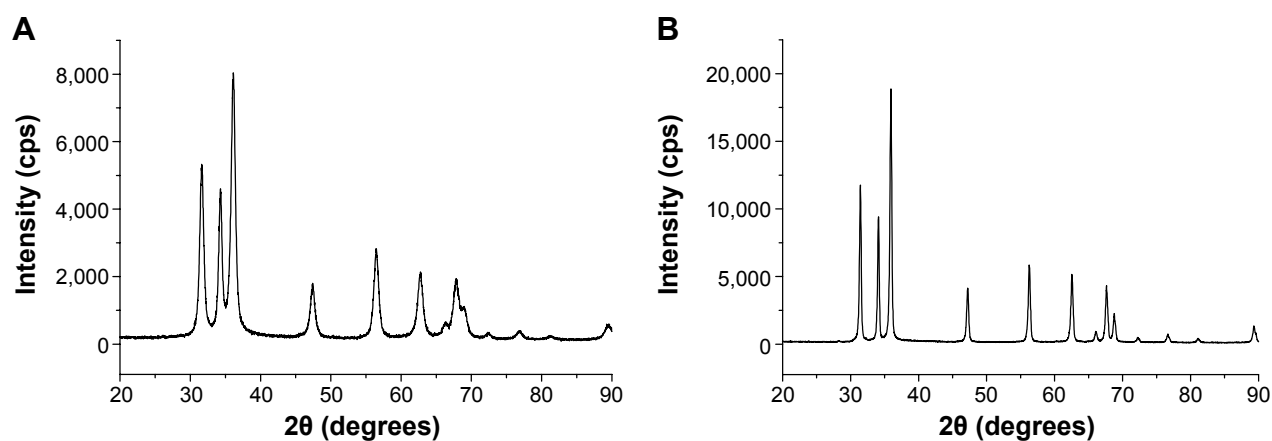
A

B

Figure S2 XRD patterns of ZnO NPs.
Notes: XRD patterns of (**A**) 10 nm and (**B**) 71 nm ZnO NPs.
Abbreviations: XRD, X-ray diffraction; NP, nanoparticle.

Table S1 Partition coefficients of 10 nm ^{65}ZnO NPs in each organ

Time (hours)	Liver	Kidney	Spleen	Lung	Brain	Heart	GI tract	Carcass
1	6.33 (4.61–8.64)	4.25 (3.24–5.64)	3.89 (1.98–6.91)	18.73 (12.28–28.01)	0.22 (0.14–0.33)	1.32 (0.86–1.94)	2.15 (1.64–2.88)	0.57 (0.41–0.77)
2	7.14 (5.46–9.31)	4.79 (3.76–6.14)	4.65 (2.89–7.18)	22.08 (14.79–32.73)	0.26 (0.18–0.35)	1.41 (0.99–1.97)	2.57 (1.99–3.38)	0.68 (0.50–0.92)
4	9.45 (7.10–12.45)	6.45 (4.91–8.44)	6.8 (4.65–9.61)	37.39 (20.11–72.16)	0.36 (0.25–0.50)	1.79 (1.23–2.48)	3.91 (2.89–5.28)	0.92 (0.63–1.27)
7	12.57 (9.88–15.87)	8.81 (7.01–11.04)	9.43 (7.08–12.28)	64.00 (33.29–127.80)	0.52 (0.40–0.68)	2.39 (1.79–3.13)	5.60 (4.32–7.23)	1.21 (0.90–1.58)
24	15.59 (12.54–19.50)	11.83 (9.68–14.43)	12.57 (9.52–16.30)	77.22 (38.98–148.80)	0.91 (0.73–1.13)	3.66 (2.99–4.44)	7.49 (5.94–9.52)	1.84 (1.48–2.26)
48	13.10 (10.96–15.70)	10.76 (9.08–12.71)	10.95 (8.61–13.84)	46.61 (25.8–84.13)	1.11 (0.91–1.34)	3.79 (3.12–4.54)	6.69 (5.49–8.17)	2.09 (1.75–2.47)
72	11.27 (9.71–13.07)	9.60 (8.41–10.97)	9.25 (7.63–11.16)	33.78 (20.18–58.07)	1.21 (1.05–1.40)	3.58 (3.05–4.16)	5.79 (4.93–6.81)	2.15 (1.87–2.45)
168	8.44 (6.90–10.30)	7.35 (6.16–8.72)	6.61 (5.40–7.95)	18.61 (12.01–29.82)	1.56 (1.25–1.92)	3.14 (2.57–3.75)	4.13 (3.44–4.94)	2.26 (1.89–2.67)
672	6.18 (4.37–8.72)	5.38 (3.90–7.36)	4.95 (3.51–6.64)	9.87 (6.33–15.63)	2.01 (1.44–2.87)	2.91 (2.05–3.98)	2.77 (2.03–3.80)	2.60 (1.87–3.45)

Note: Data presented as mean (95% CI).
Abbreviations: NP, nanoparticle; GI, gastrointestinal; CI, confidence interval.

Table S2 Partition coefficients of 71 nm ^{65}ZnO NPs in each organ

Time (hours)	Liver	Kidney	Spleen	Lung	Brain	Heart	GI tract	Carcass
1	5.91 (4.92–7.06)	3.37 (2.12–5.31)	2.37 (1.44–3.70)	3.78 (2.66–5.49)	0.05 (0.02–0.09)	0.86 (0.57–1.22)	2.33 (1.63–3.40)	0.59 (0.40–0.84)
2	6.28 (5.36–7.35)	3.52 (2.51–4.89)	2.62 (1.78–3.70)	3.93 (2.95–5.27)	0.12 (0.04–0.32)	0.99 (0.67–1.47)	2.70 (2.02–3.63)	0.66 (0.51–0.83)
4	7.33 (6.27–8.60)	4.16 (3.33–5.19)	3.43 (2.47–4.64)	4.40 (3.26–5.94)	0.28 (0.17–0.52)	1.43 (1.00–2.09)	3.85 (3.02–4.89)	0.82 (0.67–1.00)
7	8.98 (7.86–10.24)	5.39 (4.47–6.51)	4.66 (3.32–6.37)	5.55 (4.07–7.65)	0.42 (0.30–0.65)	1.96 (1.44–2.68)	5.42 (4.43–6.61)	1.09 (0.90–1.31)
24	11.50 (9.90–13.33)	7.85 (6.38–9.64)	7.00 (4.96–9.64)	7.70 (5.45–10.98)	0.73 (0.44–1.21)	3.25 (2.06–5.01)	8.10 (6.19–10.52)	2.05 (1.57–2.62)
48	10.17 (8.94–11.56)	7.34 (5.75–9.18)	6.59 (4.81–8.69)	6.65 (4.80–9.03)	0.88 (0.59–1.27)	3.46 (2.26–5.24)	7.39 (5.44–9.97)	2.40 (1.79–3.08)
72	9.20 (8.26–10.26)	6.66 (5.56–7.82)	5.87 (4.59–7.34)	5.96 (4.64–7.56)	0.95 (0.73–1.24)	3.24 (2.38–4.45)	6.51 (5.16–8.21)	2.43 (1.97–2.92)
168	8.33 (7.54–9.23)	5.72 (4.98–6.55)	4.51 (3.69–5.46)	4.98 (4.18–5.94)	1.23 (1.05–1.44)	2.86 (2.31–3.57)	5.46 (4.53–6.58)	2.70 (2.35–3.06)
672	8.77 (8.17–9.42)	5.11 (4.24–6.14)	–	3.94 (3.20–4.86)	1.80 (1.46–2.19)	–	5.17 (4.23–6.30)	4.05 (3.38–4.78)

Note: Data presented as mean (95% CI).
Abbreviations: NP, nanoparticle; GI, gastrointestinal; CI, confidence interval.

Table S3 Partition coefficients of ^{65}Zn(NO$_3$)$_2$ in each organ

Time (hours)	Liver	Kidney	Spleen	Lung	Brain	Heart	GI tract	Carcass
1	0.94 (0.58–1.51)	1.35 (0.91–2.06)	0.46 (0.26–0.76)	0.49 (0.34–0.74)	0.04 (0.03–0.06)	0.31 (0.20–0.46)	0.91 (0.59–1.44)	0.23 (0.15–0.32)
2	1.10 (0.76–1.59)	1.52 (1.11–2.13)	0.61 (0.41–0.88)	0.56 (0.41–0.78)	0.05 (0.04–0.07)	0.37 (0.26–0.51)	1.16 (0.84–1.64)	0.28 (0.21–0.36)
4	1.60 (1.24–2.05)	2.00 (1.58–2.58)	1.01 (0.77–1.31)	0.76 (0.59–0.98)	0.09 (0.07–0.11)	0.52 (0.39–0.67)	1.84 (1.44–2.34)	0.37 (0.29–0.46)
7	2.18 (1.77–2.69)	2.52 (2.03–3.16)	1.35 (1.04–1.73)	0.98 (0.80–1.23)	0.12 (0.10–0.15)	0.68 (0.53–0.87)	2.50 (2.00–3.13)	0.47 (0.29–0.58)
24	2.85 (2.30–3.53)	3.08 (2.54–3.72)	1.88 (1.41–2.53)	1.40 (1.14–1.72)	0.24 (0.19–0.30)	1.05 (0.82–1.33)	2.98 (2.42–3.72)	0.68 (0.56–0.81)
48	2.60 (2.11–3.22)	2.78 (2.35–3.30)	2.03 (1.66–2.47)	1.48 (1.23–1.80)	0.37 (0.25–0.58)	1.17 (0.94–1.44)	2.48 (2.08–2.98)	0.74 (0.63–0.86)
72	2.37 (1.92–2.94)	2.50 (2.14–2.93)	1.97 (1.67–2.31)	1.44 (1.23–1.70)	0.44 (0.29–0.72)	1.16 (0.96–1.40)	2.11 (1.80–2.49)	0.77 (0.67–0.88)
168	2.05 (1.66–2.53)	2.03 (1.66–2.48)	1.69 (1.38–2.05)	1.27 (1.04–1.55)	0.55 (0.43–0.72)	1.09 (0.86–1.35)	1.55 (1.28–1.89)	0.86 (0.71–1.03)
672	1.74 (1.23–2.46)	1.62 (1.18–2.20)	1.32 (0.94–1.78)	1.06 (0.77–1.48)	0.68 (0.48–0.94)	0.97 (0.65–1.39)	1.15 (0.85–1.59)	1.03 (0.73–1.44)

Notes: Data presented as mean (95% CI). –'s represent no estimates.
Abbreviations: GI, gastrointestinal; CI, confidence interval.

Table S4 Estimated excretion and elimination rates (h^{-1}) used in PBPK model for ^{65}ZnO NPs and ^{65}Zn(NO$_3$)$_2$ in mice

Time (hours)	Excretion and elimination rates (h^{-1})		
	10 nm ^{65}ZnO NP	71 nm ^{65}ZnO NP	^{65}Zn(NO$_3$)$_2$
Liver			
2	NE	NE	NE
4	0.0438±0.00207	0.0385±0.0234	NE
7	0.0309±0.0060	0.0382±0.0052	0.0325±0.0195
24	0.0291±0.0028	0.0292±0.0019	0.0306±0.0026
48	0.0239±0.0019	0.0264±0.0016	0.0255±0.0020
72	0.0207±0.0015	0.0240±0.0014	0.0216±0.0017
168	0.00193±0.0015	0.0234±0.0014	0.0203±0.0017
672	0.0193±0.0015	0.0234±0.0014	0.0203±0.0016
Kidney			
2	0.0618±0.0492	0.0761±0.0838	0.1218±0.0537
4	0.0287±0.0790	NE	NE
7	NE	NE	0.0614±0.0066
24	0.0166±0.0020	0.0162±0.0014	0.0389±0.0041
48	0.0131±0.0011	0.0154±0.0010	0.0309±0.0031
72	0.0122±0.0008	0.0150±0.0008	0.0260±0.0023
168	0.0106±0.0007	0.0146±0.0007	0.0253±0.0022
672	0.0106±0.0007	0.0146±0.0007	0.0252±0.0021
GI tract			
2	NE	NE	NE
4	NE	NE	NE
7	0.0321±0.0293	0.0400±0.0042	0.0629±0.0233
24	0.0238±0.0031	0.0260±0.0024	0.0508±0.0038
48	0.0197±0.0018	0.0241±0.0018	0.0445±0.0034
72	0.0179±0.0013	0.0229±0.0015	0.0415±0.0031
168	0.0168±0.0012	0.0226±0.0014	0.0414±0.0030
672	0.0168±0.0012	0.0226±0.0014	0.0414±0.0029

Note: Data presented as mean ± standard error.
Abbreviations: GI, gastrointestinal; NE, no estimates; NP, nanoparticle; PBPK, physiologically based pharmacokinetic.